Blob Detection by Relaxation

ALAN J. DANKER AND AZRIEL ROSENFELD, FELLOW, IEEE

Abstract—**A blob is a compact region lighter (or darker) than its background surrounded by a smoothly curved edge. Blobs can be detected using cooperating relaxation processes to enhance their interior and edge probabilities. A discussion of the processes working independently and together is given. The use of a pyramidal relaxation structure, the use of the closedness of contours as an additional information source, and the extension of cooperating relaxation processes to a time sequence of images are also discussed.**

Index Terms—**Blob detection, image processing, relaxation, segmentation.**

I. Introduction

BASIC to most image understanding tasks is the segmentation of objects from their background. In simple situations the objects to be extracted may be "blobs." A blob can be characterized as a compact region lighter (or darker) than its background surrounded by a smoothly curved edge. In principle, a blob can be extracted by thresholding the image at an appropriate level, or its bounds can be defined by an edge detector. However, because of noise and blur, pure object/background discrimination can rarely be achieved in this way. This paper poses a fuzzy classification scheme for blob detection. It incorporates ideas used in nonprobabilistic models making use of edge/border coincidence, and implements these ideas in the form of a probabilistic relaxation process.

In this section probabilistic relaxation is discussed and blob detection using edge/border coincidence is described.

In Section II the behavior of the edge process and the gray level process are examined, first when operating separately and then when interacting in a joint relaxation process.

Section III discusses several extensions to the blob extraction processes. These include a pyramid structure for multilevel relaxation, the use of curvature information as a basis for the initial estimation of "inside" and "outside" class probabilities, and a scheme for computing compatibility coefficients for detecting objects in a time sequence of one-dimensional images.

A. Probabilistic Relaxation

A primary step in the analysis of an image is the discrimination or classification of the parts of the image. A low level symbolic description of the image based on local evidence (i.e., gray level, gradient magnitude, curvature) can be built. However, local evidence may be misleading, causing ambiguities in the classification. Ambiguities arise from the sensitivity of local evidence to noise, or multiple responses to the same gray level pattern, as in computing slope information. The ambiguity problem is especially severe if the classification is done in parallel with each point being classified without reference to any classification decisions that may have already been made at other points. To disambiguate the classification, an iterative process which makes use of the relationships among the classes to reduce or eliminate the ambiguity is employed. This computational process is called "relaxation labeling" [1].

The relaxation labeling method uses probabilistic classification rather than making firm classification decisions immediately. Classification probabilities at a given iteration are allowed to depend on decisions made at the previous iteration. The probability updating at a given iteration is done in parallel over the entire image.

To convey the general idea of the method, a simplified overview is given in [2]. We initially assign to each point P the probability p_i that it belongs to each of its possible classes. We then examine the probabilities at neighboring points, increasing p_i if supporting evidence is found for it (i.e., if there exist high probabilities that the neighbors of P have compatible classifications), or decrease it if contradictory evidence is found (i.e., there exist high probabilities of incompatible classification at P's neighbors). The updating is then done in parallel for every P and every p_i, and the process can be iterated as many times as desired.

Two formal models of the process have been formulated and applied [3], [4]. We now briefly describe the models. Let $A = \{a_1, \cdots, a_n\}$ be the set of objects (possibly single points) in a scene, each of which belongs to one of the classes of the set $\Lambda = \{\lambda_1, \cdots, \lambda_m\}$. With each a_i we associate a probability vector $(p_{i1}, \cdots, p_{im})$, where p_{ik} is an estimate of the probability that a_i belongs to the class λ_k, where $\Sigma_{\lambda \in \Lambda} p_i(\lambda) = 1$, and $0 \leqslant p_i(\lambda) \leqslant 1$ for all $a_i \in A$. This estimate is based on some conventional analysis of a_i. For example, the initial estimate of the edgeness of the point a_i may be proportional to the magnitude of the gradient of the image at a_i. For each pair of neighboring objects a_i, a_j (given a specified neighbor relation) and each pair of classes λ_h, λ_k, there is a measure of compatibility between object a_i belonging to class λ_h and object a_j belonging to class λ_k. Compatibilities are given by the function $r_{ij}(\lambda, \lambda')$ where $-1 \leqslant r \leqslant +1$ and

1) if λ at a_i is compatible with λ' at a_j, then $r_{ij}(\lambda, \lambda') > 0$;

2) if λ at a_i is incompatible with λ' at a_j, then $r_{ij}(\lambda, \lambda') < 0$;

3) if neither labeling is constrained by the other ("don't care" situation), then $r_{ij}(\lambda, \lambda') = 0$;

Manuscript received October 22, 1979; revised January 25, 1980. This work was supported by the Defense Advanced Research Projects Agency and the U.S. Army Night Vision Laboratory under Contract DAAG-53-76C-0138 (DARPA Order 3206), and is based on A. J. Danker's M.S. thesis, University of Maryland, 1979.

A. J. Danker was with the Computer Vision Laboratory, Computer Science Center, University of Maryland, College Park, MD 20742. He is now with the Computervision Corporation, Bedford, MA 01730.

A. Rosenfeld is with the Computer Vision Laboratory, Computer Science Center, University of Maryland, College Park, MD 20742.

0162-8828/81/0100-0079$00.75 © 1981 IEEE

4) the magnitude of r_{ij} represents the strength of the compatibility.

Compatibility coefficients can be computed as correlation functions, by *a priori* evaluation of the ways in which the classes can interact, or based on mutual information of the labels at neighboring points (i.e., if two labels have a high positive correlation, it is expected that they will have a high mutual information, and vice versa). The pairwise compatibilities among the labels at adjacent points computed by mutual information are estimated using ratios of probabilities given by

$$\frac{p_{ij}(\lambda, \lambda')}{p(\lambda)\, p(\lambda')}$$

where i,j specifies a neighborhood direction and λ, λ' range over the label set. For a detailed discussion of computing compatibility coefficients by mutual information, see [5].

The new estimate of the probability of λ at a_i at the $(k+1)$st iteration is a function of both the previous estimate for that probability, $p_i^k(\lambda)$, and the contribution from the probability distributions on the neighboring label sets, $q_i^k(\lambda)$, $\forall \lambda \in \Lambda$, given by [3]

$$p_i^{(k+1)}(\lambda) = \frac{p_i^k(\lambda)\,[1 + q_i^k(\lambda)]}{\sum_\alpha p_i^k(\alpha)\,[1 + q_i^k(\alpha)]}$$

where

$$q_i^k(\lambda) = \sum_j \sum_\alpha r_{ij}(\lambda, \alpha)\, p_j(\alpha).$$

This updating scheme is useful when compatibilities are expressed as positive and negative coefficients. When compatibilities are computed by mutual information a nonnegative coefficient scale results, where 0 represents high incompatibility and high values represent high compatibilities. The second model works with these compatibilities. The new estimate of the probability of λ at a_i at the $(k+1)$st iteration is given by [4]

$$p_i^{(k+1)}(\lambda) = \frac{p_i^k(\lambda) \sum_\alpha r_{ij}(\lambda, \alpha)\, p_j^k(\alpha)}{\sum_\lambda \sum_\alpha r_{ij}(\lambda, \alpha)\, p_i^k(\lambda)\, p_j^k(\alpha)}.$$

When the α's at a_j are highly compatible with $p_i(\lambda)$ the sum will be high, low otherwise, and $p_i(\lambda)$ will increase relative to other p's.

Both iteration schemes yield comparable results. A study of the convergence properties of relaxation processes is found in [6], [7]. Relaxation methods have been used in breaking substitution ciphers [8], handwriting segmentation [9], [19], line and curve enhancement [1], [10], [11], and edge enhancement [12], [13], among other applications.

B. Blob Detection

Segmentation of objects from their background is basic to many image understanding tasks. This paper deals with the relatively simple case in which the object is a "blob." A blob can be characterized as a compact region lighter (or darker) than its background surrounded by a smoothly curved edge. Not all images conform to this rudimentary model; for example, consider images of clouds whose regions lack well defined outlines, or images that consist of subparts with differing textures. However, the model is applicable to many imaging tasks including thermal imagery analysis, chromosome classification, and industrial automation.

In principle, blobs can be extracted by thresholding the image at an appropriate level. However, if the image is noisy, thresholding will produce noisy results which may not be cleaned up in postprocessing. Thresholding may extract regions that are not bounded by edges but are smooth continuations of the background if the gray level fluctuations in the background cross the threshold level. Edge detection is also sometimes useful in object extraction. However, the edge detector may respond in the interior of the object or background as a result of noise or may fail to respond strongly on the object/background border because of blur.

Milgram [14], [15] has investigated the use of edge/border coincidence as a method for object detection using the "superslice" algorithm. The basic concept is the matching of border points of connected components with corresponding edge values. In this approach, an edge detector is run over the image and the response thinned to an "edge map." The image is then thresholded and connected components of above-threshold points are extracted (see Rosenfeld and Kak [16] for a discussion of connected components and edge detectors). The components are accepted as objects or rejected as noise based on the coincidence of the edge map with the region boundary. This process is carried out at various thresholds and at each threshold the surviving regions are compared with the survivors of earlier thresholds. Only those regions that best match the edge map are used to describe the actual objects in the image.

Nakagawa used edge/border coincidence as an aid in edge extraction [17]. He was able to reduce the noisiness in the edge detector response by selecting those edge points that lie on region borders in the thresholded image. The selected edge points were linked into continuous curves by following the region borders.

Parikh experimented with the use of border edge strength values to determine a threshold for cloud-type objects [18]. Edge strength was defined to be the sum of the edge values for all border points of a given connected component divided by the number of border points. The border edge strength feature failed to segment the cloud-type objects because of the ill-defined nature of the borders.

Relaxation applied to the detection of edges was successfully investigated by Schachter *et al.* [12]. In their approach, the gradient magnitude was computed by

$$\mathrm{MAG} = \sqrt{(\Delta_x F)^2 + (\Delta_y F)^2}$$

where F is the image and $\Delta_x F$, $\Delta_y F$ are the x, y components of the gradient, respectively. The edge direction was given by

$$\theta = \tan^{-1}\left(\frac{\Delta_y F}{\Delta_x F}\right).$$

The probability of an edge at a point (x, y) was defined by

$$p(x,y) = \frac{\mathrm{MAG}(x,y)}{\max\limits_{u,v} \mathrm{MAG}(u,v)}$$

where the max was taken over the entire image. $\overline{P}(x,y) = 1 - P(x,y)$ defined the no-edge probability. Edge/edge compatibility coefficients were computed based on smoothness of slope continuation for edge/edge; edge/no edge and no edge/no edge interactions were also defined. In brief, no edge reinforces no edge; edge reinforces edge if they smoothly continue one another; and edge reinforces no edge if they are alongside one another.

To apply relaxation to thresholding [21], "light" and "dark" probabilities are initially assigned to image points based on their gray levels. The probabilities are iteratively adjusted at each point based on the probabilities at the neighboring points, i.e., light reinforces light and dark reinforces dark. This has the effect of shifting the probabilities initially assigned to noise points so as to make them more consistent with their surroundings. After a number of iterations, light probabilities should become uniformly high, and vice versa, producing a bimodal histogram with peaks at opposite ends of the gray scale, making threshold selection easier and resulting in a nonnoisy binary image. However, the process still may extract regions not bounded by edges.

This paper uses the ideas of relaxation and the ideas of edge/border coincidence in a probabilistic segmentation scheme for blob detection. Superslice, a nonprobabilistic scheme, made two independent decisions based on gray level (thresholding) and edge strength (selection of maxima), then checked for coincidence to determine if an object was detected. The joint relaxation process described in this paper, on the other hand, never makes decisions. It estimates the probabilities based on gray levels and edge strengths, and then iteratively adjusts these probabilities so that both types of information are able to interact. This process thus incorporates the principle of convergent evidence in a deferred commitment scheme.

II. Blob Detection

In this section we examine the edge and gray level processes operating separately, and then the joint process in which they are both combined.

A. Edge Relaxation

We compute the initial edge probabilities as follows. Let $e_i (i = 1, \cdots, 8)$ be a measure of the gray level difference at point P in direction $45i^\circ$, where e_i is computed by applying these masks, first proposed by Prewitt, at every picture point:

$$\begin{matrix} -1 & 0 & 1 \\ -1 & P & 1 \\ -1 & 0 & 1 \end{matrix} \qquad \begin{matrix} 0 & 1 & 1 \\ -1 & P & 1 \\ -1 & -1 & 0 \end{matrix} \qquad \begin{matrix} 1 & 1 & 1 \\ 0 & P & 0 \\ -1 & -1 & -1 \end{matrix} \qquad \begin{matrix} 1 & 1 & 0 \\ 1 & P & -1 \\ 0 & -1 & -1 \end{matrix}$$

We take the absolute value as the edge magnitude and let the sign indicate the edge orientation (i.e., a 90° edge is a negative 270° edge). The operator has the effect of thickening edges, i.e., producing edge responses on the leading and trailing sides of the object border. To obtain usable edge information, the output must be thinned by suppression of nonmaxima of the edge magnitude in the direction across the edge at each point.

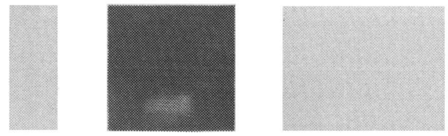

Fig. 1. FLIR image of tank.

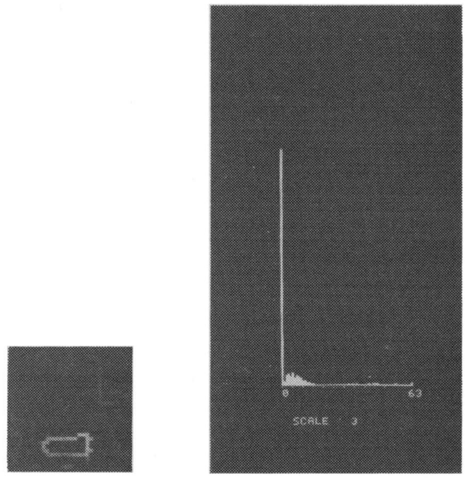

(a) (b)

Fig. 2. (a) Edge detector response to Fig. 1. (b) Histogram of edge strengths.

Fig. 1 shows the FLIR image of a tank displayed as gray levels. Fig. 2(a) shows the edge detector output with nonmaximal responses suppressed. This illustrates the problem of the edge detector responding to varying intensity patterns in the background. A histogram of the edge strengths is shown in Fig. 2(b).[1]

Let E be the largest e value at any point of the image, and let e_P be the largest value at point P. $p_e = e_P/E$ is taken to be an estimate of the edge probability at P and $p_n = 1 - p_e$ as an estimate of the no edge probability. Further, $p_i = (e_i/s)\, p_e$, where $s = \sum_{i=1}^{8} e_i$, is taken as an estimate of the probability of an edge in direction $45i^\circ$ at P. Thus, $\sum_{i=1}^{8} p_i = p_e$ and $p_e + p_n = 1.0$. Fig. 3(a) shows the initial edge classifications with pixels having maximum edge probability (regardless of direction) rescaled as gray levels between 0 and 63, and pixels having maximum no edge probabilities displayed as black.

The pairwise compatibilities among $p_1, \cdots, p_8, p_n$ at adjacent points are estimated using mutual information [5]. A few of the coefficients are shown in Fig. 4, showing that the relative strengths of the coefficients support the intuitive constraints of no edge reinforcing no edge, edge reinforcing edge if they smoothly continue one another, and edge reinforcing no edge (and vice versa) if they are alongside one another. This has the effect of strengthening the appropriate edge probabilities at points that lie along smooth edges, and strengthening the no edge probability elsewhere. These coefficients are used in the relaxation process of [4].

[1] The scale in all histogram pictures indicates the number of pixels per displayed dot.

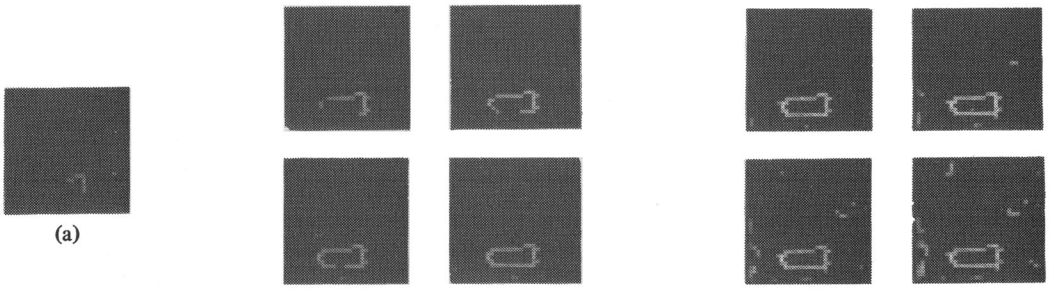

(a) (b)–(e) (f)–(i)

Fig. 3. (a) Initial edge/no edge classifications of Fig. 1. (b)–(i) Eight iterations of relaxation applied to Fig. 3(a).

label[p] : →	label[nbr] : →		label[p] : →	label[nbr] : ↖	
3. 449571	2. 735268	2. 989768	0. 618779	1. 834991	0. 656950
13. 303496	p	13. 303496	0. 094431	p	0. 600613
2. 989768	2. 735268	3. 449571	0. 137451	0. 153977	0. 163758

label[p] : →	label[nbr] : ←		label[p] : →	label[nbr] : ↗	
0. 069581	0. 219511	0. 164322	1. 907638	4. 107503	4. 381657
0. 002263	p	0. 003521	8. 935122	p	10. 084600
0. 030989	0. 045222	0. 031845	2. 596691	2. 433852	2. 016059

label[p] : →	label[nbr] : ↑		label[p] : →	label[nbr] : ↙	
1. 036540	4. 441962	3. 797525	1. 078657	0. 947074	0. 652277
1. 751447	p	3. 200273	0. 200243	p	0. 129268
0. 914150	1. 432359	0. 398709	0. 025246	0. 162744	0. 088019

label[p] : →	label[nbr] : ↓		label[p] : →	label[nbr] : NE	
4. 106131	2. 371873	1. 064473	0. 868406	0. 891125	0. 875631
4. 828966	p	3. 729727	0. 686561	p	0. 674626
0. 525983	1. 328874	1. 809332	0. 919590	0. 954691	0. 906917

label[p] : →	label[nbr] : ↘	
4. 723255	2. 132231	0. 993537
12. 241382	p	11. 387216
2. 307259	2. 240219	3. 518801

Fig. 4. Examples of compatibility coefficients for edge relaxation. The edge → is a $\xrightarrow[\text{dark}]{\text{light}}$ edge with the other edges rotations of it.

Fig. 3(b)–(i) shows eight iterations of the edge relaxation process applied to Fig. 3(a). Fig. 5(a)–(i) are the histograms of the respective iterations. As the relaxation process iterates the edge responses clustered at the lower end of the scale in Fig. 2(b) migrate in two directions. Those points which have low edge support have increased no edge probabilities and become zero while those points receiving support have increased edge probabilities and move toward the higher values. The no edge points show up as a spike at gray level zero. The blob edge becomes significantly enhanced with the blob being completely defined after four iterations. As the process continues some of the edges in the background begin to come out; however, the improvement over Fig. 2(a) is obvious.

B. Light/Dark Relaxation

The light/dark process was initially designed as an automated thresholding process wherein the gray levels would decide whether they belonged to the light class or dark class. The result should be a bimodal histogram, which makes threshold selection obvious. (See [21] for a discussion of thresholding using light/dark relaxation.) In the image domain with which we are experimenting, involving homogeneous objects on a contrasting background, the light class can be equated with blob interior and the dark class with blob exterior. As it relates to edge/border coincidence, this process has the joint role of supplying the border information and classifying the object interior. The border is defined by interior points on the light sides of edges. However, we first examine the behavior of the process without the edge interaction.

We compute the initial light/dark probabilities as follows. Let g be the gray level of point P, and let b, w be the lowest and highest gray levels in the image, so that $b \leqslant g \leqslant w$ for all P. $p_w \equiv (g - b)/(w - b)$ is taken as the estimate of the probability that P is white, and $p_b \equiv (w - g)/(w - b)$ as the probability that P is black. Fig. 6(a) shows the initial light/dark classifications of Fig. 1 redisplayed as gray levels where

$$g = b + p_w(w - b) = w - p_b(w - b).$$

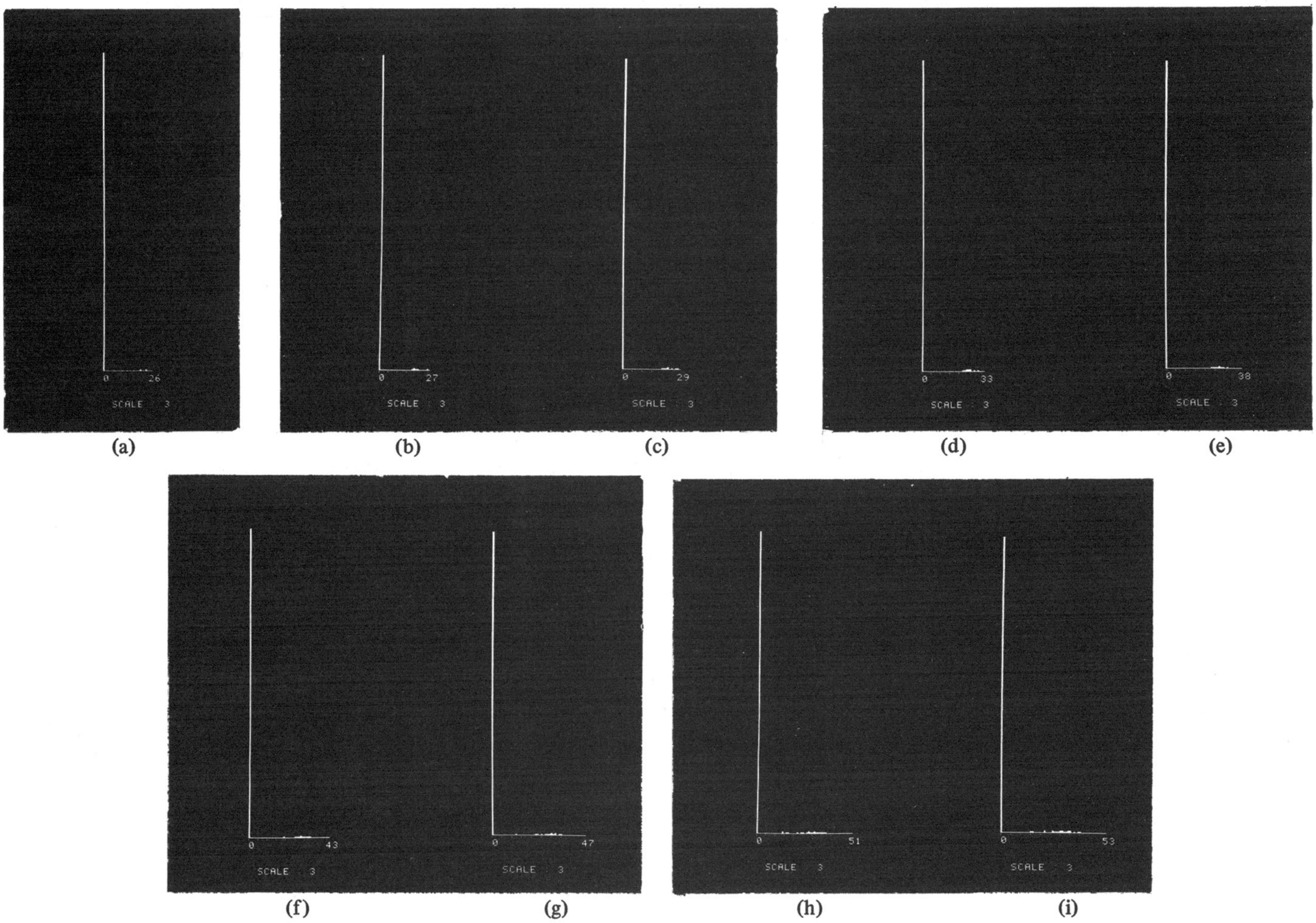

Fig. 5. (a)–(i) Histograms of Fig. 3(a)–(i).

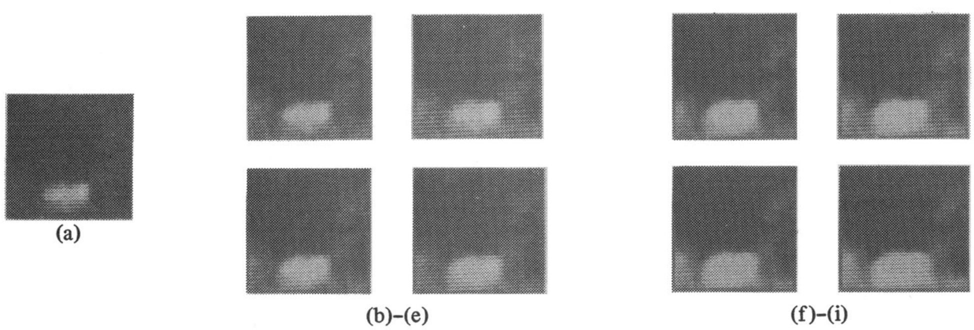

Fig. 6. (a) Initial light/dark classifications of Fig. 1. (b)–(i) Eight iterations of relaxation applied to Fig. 6(a).

Because the intial probabilities are based on gray levels and then redisplayed as gray levels, Fig. 6(a) is a copy of the original image.

The compatibilities between the black and white classes at adjacent points are estimated using ratios of average probabilities, as in the previous section. Fig. 7 shows a few of these compatibilities; we see that interior reinforces interior, exterior reinforces exterior, and adjacent interior/exterior classes are contradictory.

Fig. 6(b)–(i) shows eight iterations of the relaxation process applied to Fig. 6(a). Displayed in this figure is the strength of each point's light classification. This is interpreted as the probability that each point belongs to the interior class. As the process iterates the blob interior grows. After three iterations those ambiguously classed points on the blurred edge become classified as interior. However, with no inhibitory process to temper this growth, background points neighboring the blob interior begin to accept the interior support and become classified as interior themselves. Some areas in the background which do not look blob-like (lacking smoothly curving edges) have also been somewhat enhanced. This is due to their relatively high gray level and the fact that supporting evidence is based only on gray level.

Fig. 8(a)–(i) show the histograms of the corresponding itera-

label[p] : Light label[nbr] : Light			label[p] : Dark label[nbr] : Light		
1. 899474	1. 911622	1. 861720	0. 878841	0. 863841	0. 872712
1. 908425	p	1. 889212	0. 833591	p	0. 825634
1. 802868	1. 831607	1. 800759	0. 809413	0. 792967	0. 799459

label[p] : Light label[nbr] : Dark			label[p] : Dark label[nbr] : Dark		
0. 823850	0. 821471	0. 831243	1. 023727	1. 026665	1. 024928
0. 822097	p	0. 825860	1. 032589	p	1. 034147
0. 842769	0. 837141	0. 843182	1. 037324	1. 040545	1. 039273

Fig. 7. Compatibility coefficients for light/dark relaxation.

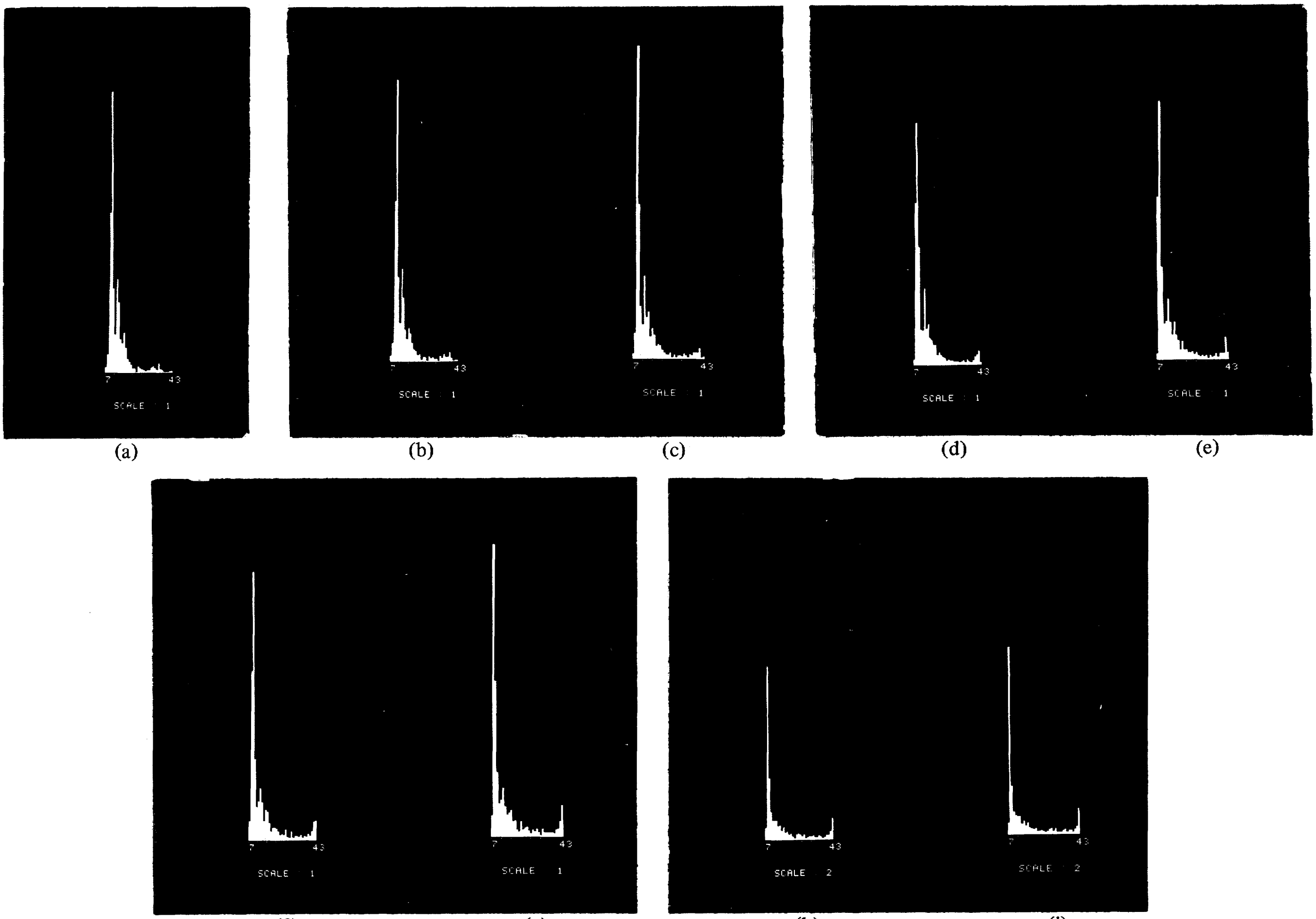

(a) (b) (c) (d) (e) (f) (g) (h) (i)

Fig. 8. Histograms of Fig. 6(a)–(i).

tions shown in Fig. 6(a)–(i). The process produces a discrimination between the blob and the background evident by the widening valley between the exterior class, peaked at the low end of the histogram around gray level seven, and the interior class peak gaining strength around gray level 43. A difference between the objective of this process and the thresholding process is that this produces no segmentation since no actual thresholding has been done.

C. Joint Relaxation

We now allow both information sources to interact in a multiprocess relaxation scheme. Given the two initial sets of probabilities for each point, compatibility coefficients can be defined between $p_b, p_w, p_1, \cdots, p_8, p_n$ in the same manner as in the previous sections. The edge/border interaction is embodied in the interprocess compatibilities where edge reinforces light if it is on the light side of the edge (and vice versa), edge reinforces dark if it is on the dark side of the edge (and vice versa), and the no edge/(light, dark) iterations are "no information" situations. The intraprocess compatibilities preserve the same reinforcement relations as previously detailed. Fig. 9 is a sampling of these coefficients.

We compute adjusted probabilities using the relaxation formula by allowing the classes to interact as before but normalizing the two sets separately. At each iteration the updated light/dark estimates are normalized by

label[p] : Light	label[nbr] : →		label[p] : Dark	label[nbr] : →	
0.935456	0.979661	0.941326	0.988469	0.994717	0.960597
0.814138	p	0.825806	1.709483	p	1.659618
0.638911	0.652284	0.641232	2.455052	2.620640	2.460205

label[p] : Light	label[nbr] : ↑		label[p] : Dark	label[nbr] : ↑	
0.932524	0.803443	0.607502	1.199085	1.884802	2.240233
0.947256	p	0.585945	1.237704	p	2.469181
0.900551	0.770539	0.580406	1.217793	1.898205	2.286948

label[p] : Light	label[nbr] : ↘		label[p] : Dark	label[nbr] : ↘	
0.886375	0.987558	1.002437	1.119594	0.979270	0.820992
0.758947	p	0.920270	1.849878	p	1.320164
0.602609	0.700845	0.756032	2.487267	2.366656	1.997890

label[p] : Light	label[nbr] : ↙		label[p] : Dark	label[nbr] : ↙	
0.610647	0.699178	0.757497	2.559976	2.421634	2.103482
0.719115	p	0.872555	2.120563	p	1.616848
0.748469	0.841446	0.855027	1.534926	1.373878	1.270607

label[p] : Light	label[nbr] : NE		label[p] : Dark	label[nbr] : NE	
0.943953	0.978146	0.945335	0.880897	0.902736	0.877210
0.974432	p	0.975667	0.927173	p	0.924237
0.941775	0.975762	0.942862	0.901072	0.923959	0.897943

Fig. 9. Examples of compatibility coefficients for joint relaxation.

$$p_l = \frac{p_l'}{p_b' + p_w'}$$

where $l = b$ or w and p_l' is the updated unnormalized estimate of l, and the updated edge estimates by

$$p_k = \frac{p_k'}{p_1' + \cdots + p_8' + p_n'}$$

where $k = (1, \cdots, 8, n)$.

Fig. 10(a)–(i) shows the results of the initial classification and eight iterations of the joint relaxation process applied to Figs. 3(a) and 6(a). The figure consists of a pair of images for each iteration. In one p_w is displayed and in the other p_e is displayed. Allowing both sources of information to interact has sped up the blob edge definition. Operating in isolation, as in Fig. 3, four iterations were needed to define the blob completely. Operating jointly, only three iterations are needed. The edges which come out of the background in the single process are greatly inhibited in the joint process. A comparison of Figs. 2(a), 3(i), and 10(i) (edge) shows a dramatic improvement. One shortcoming of the light/dark process operating alone was the blob's growth into the background. As a result of interacting with the edge information this expansion is contained, yet not entirely inhibited outside of the defined edge. The containment is most observable in the latter iterations of the process. The emergence of white patches from the background not bounded by edges is unimproved by the increased information. This is because, as can be seen from the edge process alone, there are edges in the background giving support to the light class on the light side of the edge, and no-edge probabilities have no inhibitory effect on either the light or dark probabilities.

The histograms of Fig. 10(a)–(i) are shown in Fig. 11(a)–(i). The effect of the joint process on the light/dark classifications can be analytically supported by a comparison of the light/dark process histograms of this figure with the histograms of the light/dark process operating alone (Fig. 8). The light/dark peaks are separated by a much sharper valley in the joint process, meaning that fewer points are ambiguously classified (relatively equal light/dark probabilities) and thus there is greater discrimination between the object and the background. The effect of the joint process on the edge/no edge classification can also be analyzed in the light of a comparison of the edge process histograms of this figure and the histograms of the edge process operating alone (Fig. 5). Although the strongest edge in the joint process is weaker than in the single process, the bulk of the edges are stronger, and the ambiguously classified edges, appearing around the low middle gray levels in the single process histogram, have been eliminated. This reflects the inhibition of edges in the background as seen in the joint gray level display.

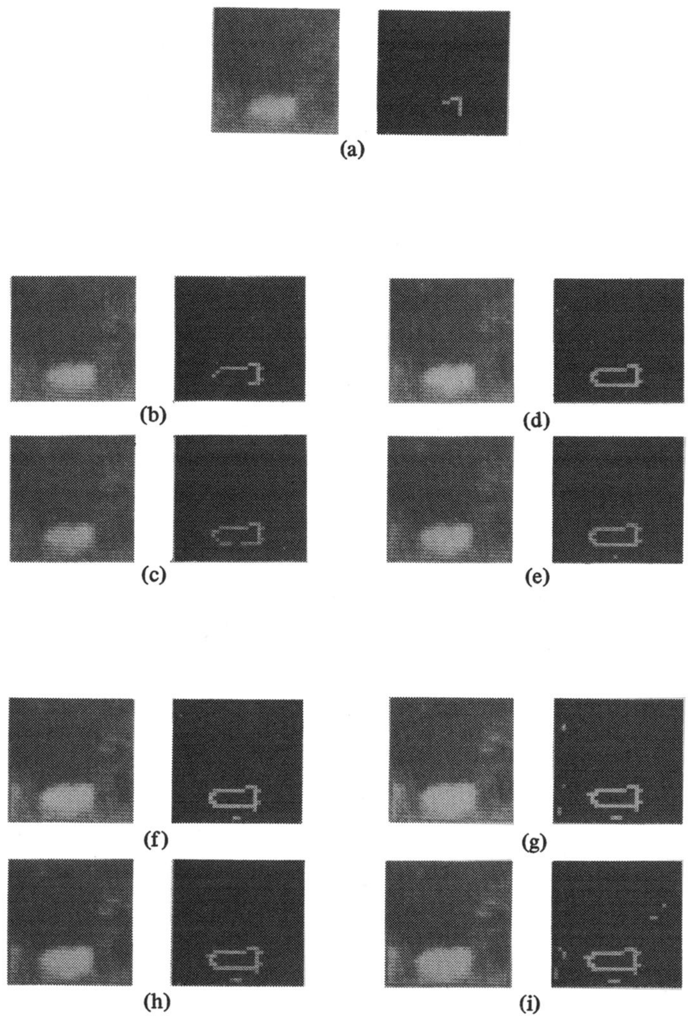

Fig. 10. (a) Initial (edge/no edge)/(light/dark) classifications of Fig. 1. (b)–(i) Eight iterations of relaxation applied to Fig. 10(a).

A modification to the joint relaxation process was tried in order to deal with the problem of the blob's growth into the background. p_b and p_w are initialized based on a "borderness" measure, where p_w is initially high only adjacent to the light sides of edges and low elsewhere. (The idea that the human visual system "colors in" regions based on gray levels adjacent

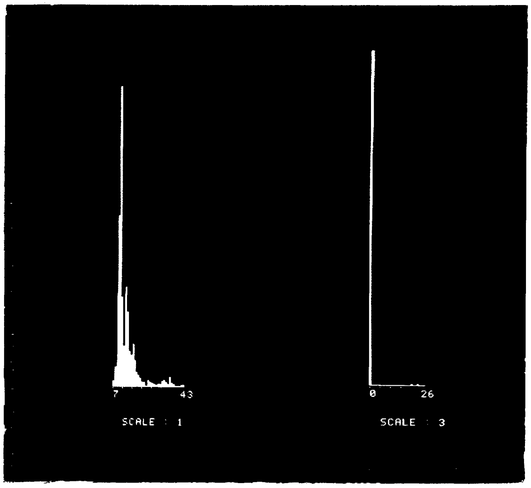

(a)

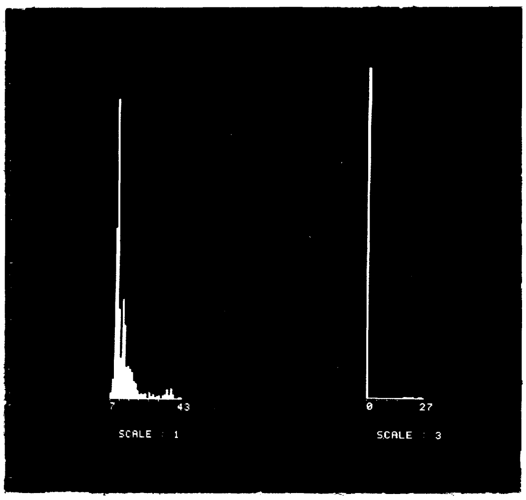

(b)

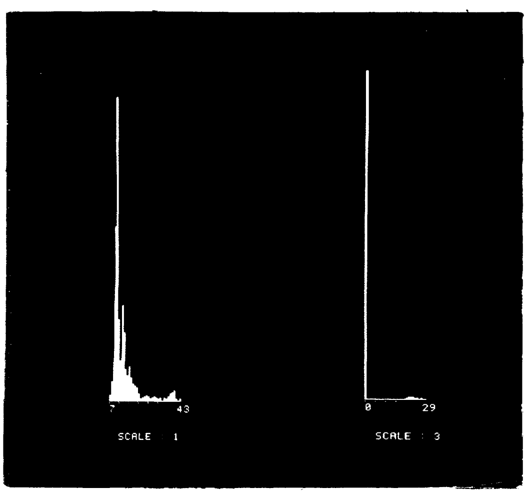

(c)

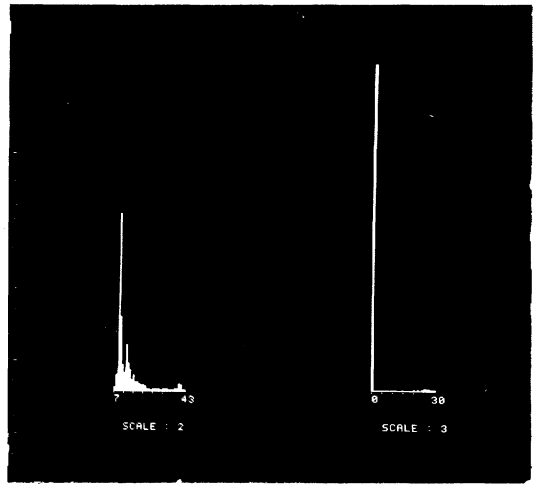

(d)

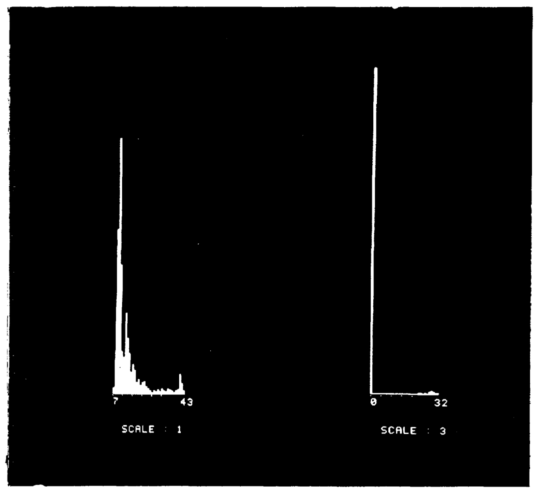

(e)

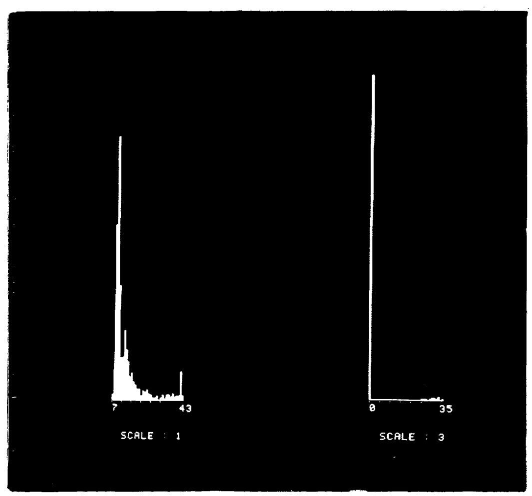

(f)

Fig. 11. (a)–(i) Histograms of Fig. 10(a)–(i).

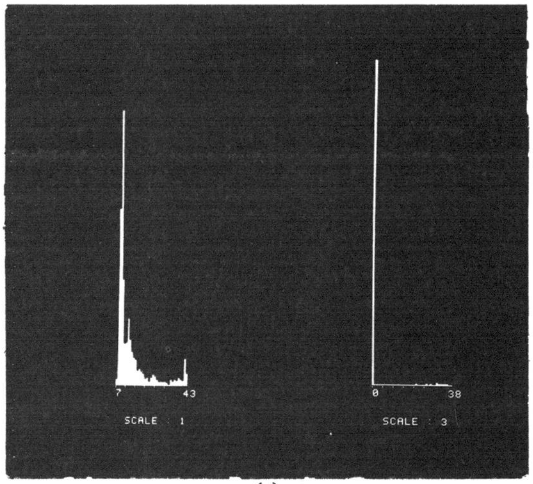

(g)

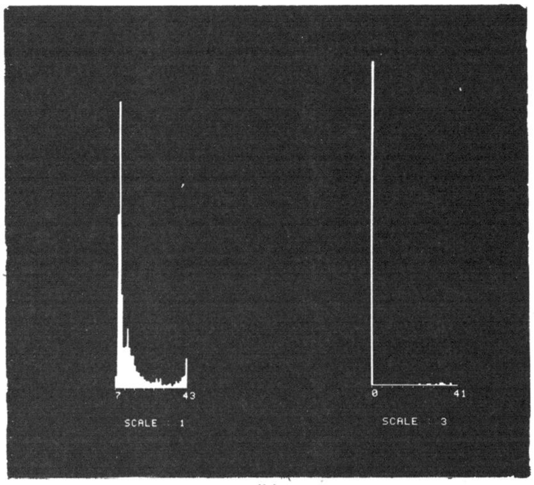

(h)

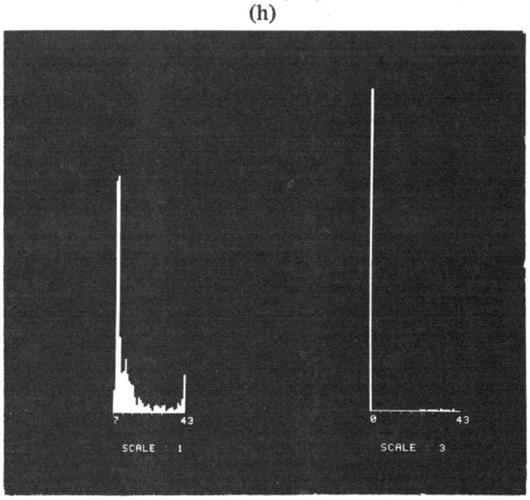

(i)

Fig. 11. *Continued.*

to their edges is well known to perception psychologists [22].) Borderness values are computed by adding the difference value e_i (the result of applying each mask) to the points marked by 1's if $e_i > 0$, or the absolute value of e_i to the points marked by -1's if $e_i < 0$, in each of the masks shown in the previous section. The result is a set of "borderness" values which are high on the light sides of edges and low elsewhere.

p_b and p_w are initialized based on a combination of the gray

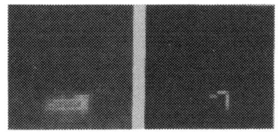

(a)

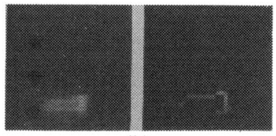

(b)

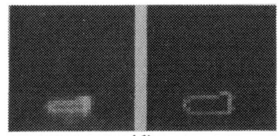

(d)

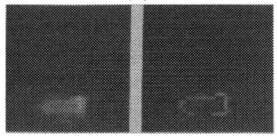

(c)

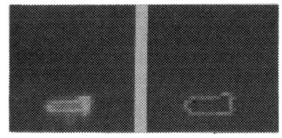

(e)

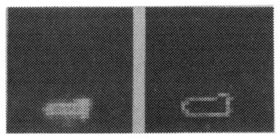

(f)

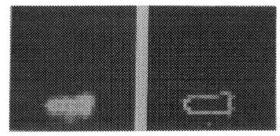

(h)

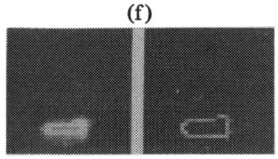

(g)

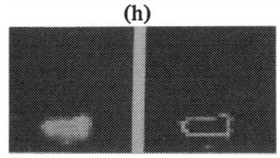

(i)

Fig. 12. (a) Initial borderness classifications to Fig. 1. (b)–(i) Eight iterations of relaxation applied to Fig. 12(a).

level and the borderness values at each point. Let B be the maximum borderness value in the image. Let β be the borderness value at point P, and let $p_\beta = \beta/B$. Let $p_w^* \equiv \alpha p_w + (1 - \alpha) p_\beta$, where $0 \leqslant \alpha \leqslant 1$ and p_w is computed as before, and let $p_b^* \equiv 1 - p_w^*$.

With the edge initialization, compatibility coefficients and the relaxation process carried out as in the joint process, Fig. 12(a)–(c) show the results of the initial classification and eight iterations with $\alpha = 0.5$. This is an obvious improvement over the results in Fig. 10. The object definition is sharper and the emergence of light patches from the background has been effectively inhibited. Improvement has also been made in the edge classifications. The histograms of this process, Fig. 13(a)–(i), support what is observable in the gray level display.

III. Extensions

Several extensions of the blob extraction process have been considered. Two of these, involving multiple-resolution images ("pyramids") and time sequences of images, are briefly discussed in the next section. This section discusses other possible sources of information that can be used as aids in blob detection.

An additional information source investigated was the use of curvature as a basis for initial estimation of "inside" and "out-

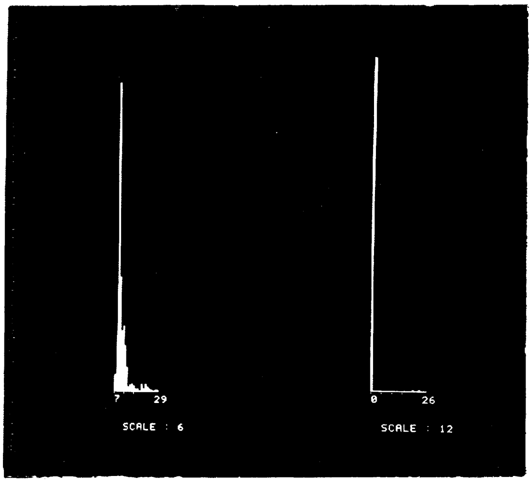

(a)

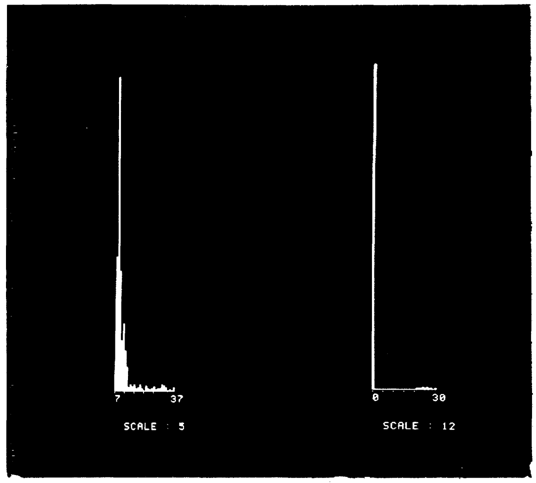

(d)

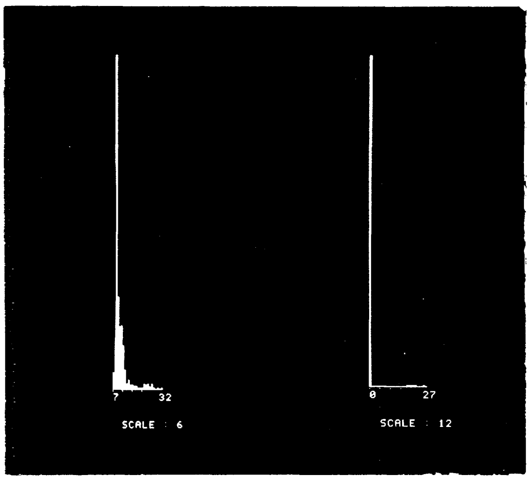

(b)

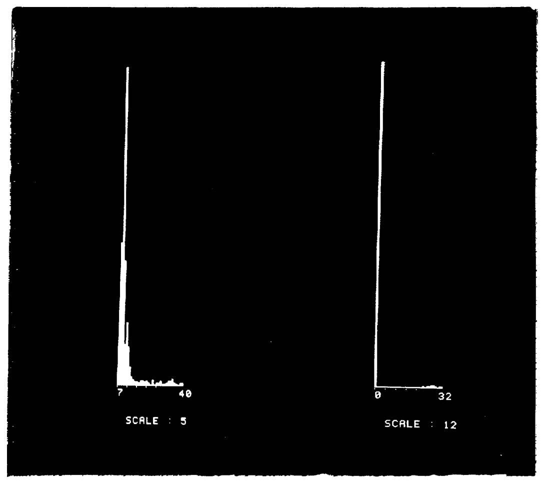

(e)

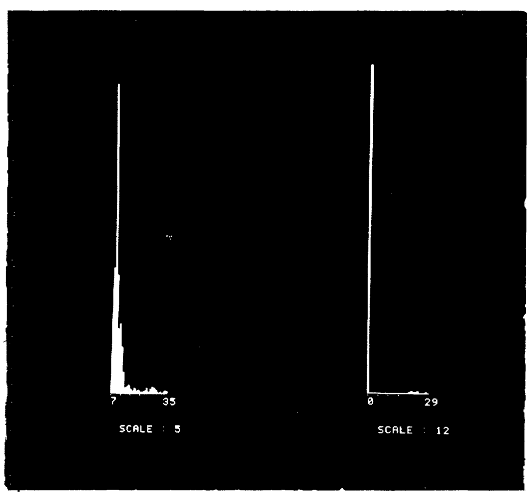

(c)

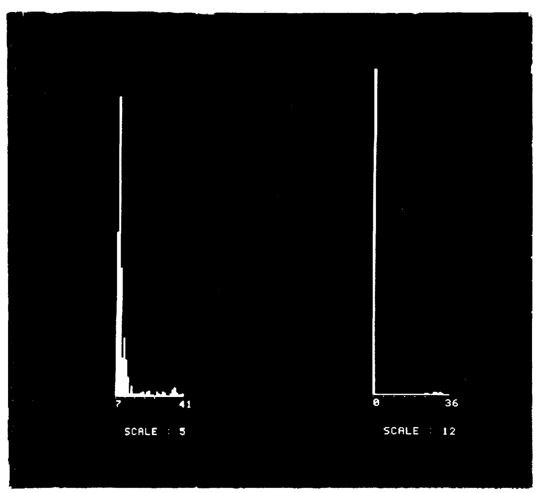

(f)

Fig. 13. (a)–(i) Histograms of Fig. 12(a)–(i).

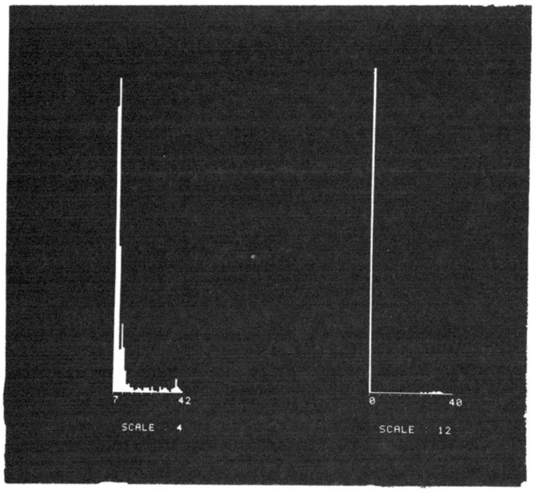

(g)

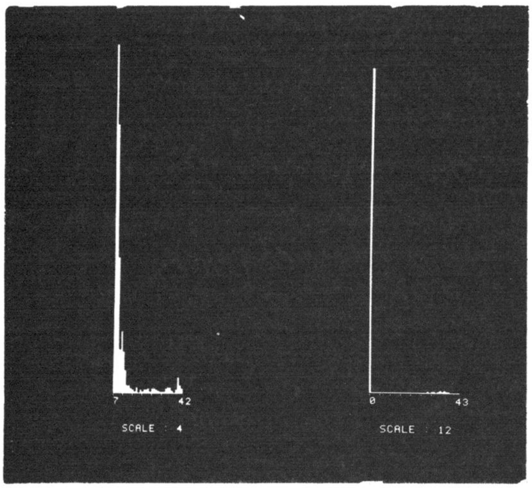

(h)

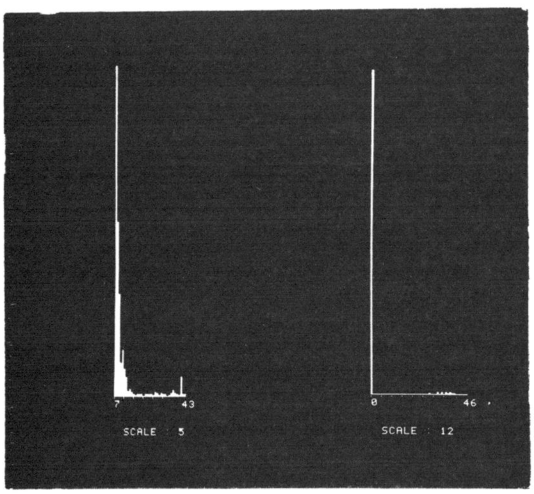

(i)

Fig. 13. *Continued.*

side" class probabilities to augment the "light" and "dark" classes in object interior/exterior interpretation. Initially, most points have equal probability of being inside or outside (assuming we do not know whether the blobs are light and the background dark or vice versa), except that points adjacent to an edge on the side away from the center of curvature have higher probability of being outside while those points on the side toward the center of curvature have higher probability of being inside. These probabilities then reinforce one another; inside reinforces inside and outside reinforces outside for neighboring pairs of points to the extent that they are not separated by an edge. Initially, the probabilities at a given point adjacent to the blob border will depend on whether the border is convex or concave at that point. Eventually, the interior of the blob should be uniformly labeled "inside" and the exterior labeled "outside" with high probability. This method can be used to label the interior of a closed curve even if it does not differ in gray level from the exterior.

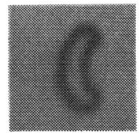

Fig. 14. Curve.

A hand-drawn kidney bean shaped closed curve was used to demonstrate the method; see Fig. 14. The curve was chain-coded and curvature at each point was measured by computing two slope vectors four chain links in length, one on each side of the point, normalizing each by its magnitude and taking the dot product of the vectors [20]. Using four-neighbor adjacency, those points adjacent to the edge which were toward the center of curvature were labeled "inside," and those points adjacent to the edge but away from the center of curvature were labeled "outside." The probability of belonging to each class was computed by normalizing the curvature measure at the adjacent edge by the maximum curvature value possible. If a point was adjacent to more than one edge point, supporting curvature evidence (i.e., all adjacent edge points were either convex or concave) increased class probability in proportion to the evidence strength, while contradictory curvature evidence (i.e., adjacent edge points having convex and concave measurements) created an ambiguous situation and inside/outside class probabilities were set equal. Points not adjacent to an edge were also initially assigned ambiguous, equal inside/outside probabilities. In this experiment, the edge points are known so no fuzzy classification was necessary. Edge points were assigned an edge probability of 1 and all other points assigned a 0 edge probability. Fig. 15(a) shows the initial pixel classifications with the class probabilities rescaled as gray levels where $g = 63 - p_I * 63 + 0.5 = p_0 * 63 + 0.5$. Initially, most points are ambiguously classified and appear gray.[2]

The compatibility coefficients for the relaxation process were determined *a priori* based on the constraints that inside reinforces inside and outside reinforces outside; an inside/outside label pair is contradictory, and classes separated by an edge do not interact. They are displayed in Fig. 16.

Fig. 15(b)-(m) shows 12 iterations of relaxation applied to Fig. 15(a). In this display scheme, as class support increases, the inside class goes to black, the outside class goes to white, and the curve remains gray. As expected, the ambiguity is re-

[2]It should be pointed out that the high and low initial values at the bottom of the concavity on the right side seem to be reversed.

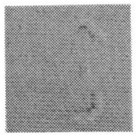

(a)

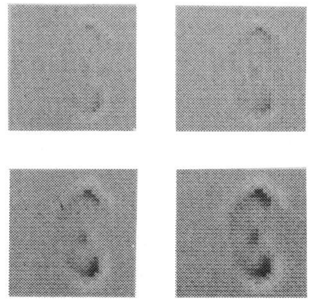

(b)–(e)

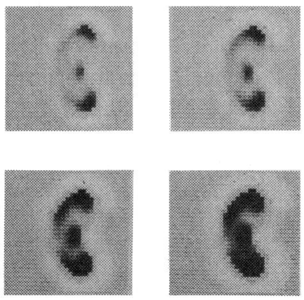

(f)–(i)

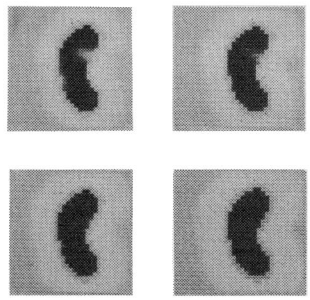

(j)–(m)

Fig. 15. (a) Initial inside/outside classifications of Fig. 14. (b)–(m) Twelve iterations of relaxation applied to Fig. 15(a).

Inside	Inside	6.0
Inside	Outside	0.
Inside	Edge	.5
Outside	Inside	0.
Outside	Outside	6.0
Outside	Edge	.5
Edge	Inside	.5
Edge	Outside	.5
Edge	Edge	.5

Fig. 16. Compatibility coefficients for inside/outside relaxation.

solved with the interior of the curve classified "inside" and the exterior classified "outside." The histograms of the iterations, Fig. 17(a)–(m), show the behavior of the process. Initially, nearly all points are ambiguously classified and show up as a spike at the middle of the histogram (at value 32). As the process iterates, the spike separates with the inside class points migrating to 0 and the outside class points migrating to 63. The exterior points beyond the outwardly propagating wavefront of "outside" support and the curve points themselves remain ambiguously classified. If the process were iterated further, the entire exterior would be classified "outside" and the histogram would then consist of three spikes: an "inside" class spike at 0, and "outside" class spike at 63, and a small curve spike at 32.

Processes of this type might be used to model figure-ground ambiguity, such as the Rubin vase, by initiating a propagation process at some particular sharply curved part of the boundary between the two regions.

IV. Conclusion

We have examined a fuzzy classification scheme for blob detection which bases its classification updating on edge and gray level information. We examined the processes operating both independently and together. We also discussed extensions to these processes and to the problem domain.

The edge relaxation process operating independently defined the object after four iterations, but with some edges being brought out of the background as the process continued. However, the results were an improvement over the nonprobabilistic edge detector results. Interacting with the light/dark information resulted in further inhibition of the background edges that did not surround a blob, and yielded complete blob definition in fewer iterations. The borderness scheme further improved the results producing an almost perfect segmentation.

In the light/dark relaxation process operating independently the blob interior grew into the background. Interaction with the edge information substantially contained the interior growth and produced an improved object/background discrimination. In the borderness scheme the object interior grew inwards filling the object and resulting in a further object/background discrimination.

Under the premise that multilevel processes have faster information propagation and are more informed than single level processes we tried relaxation on a pyramid structure of successively resolved images. As this was the first stage of experimentation, we tried the default option of computing compatibility coefficients by mutal information. The results were no improvement over the single level process. The next step ap-

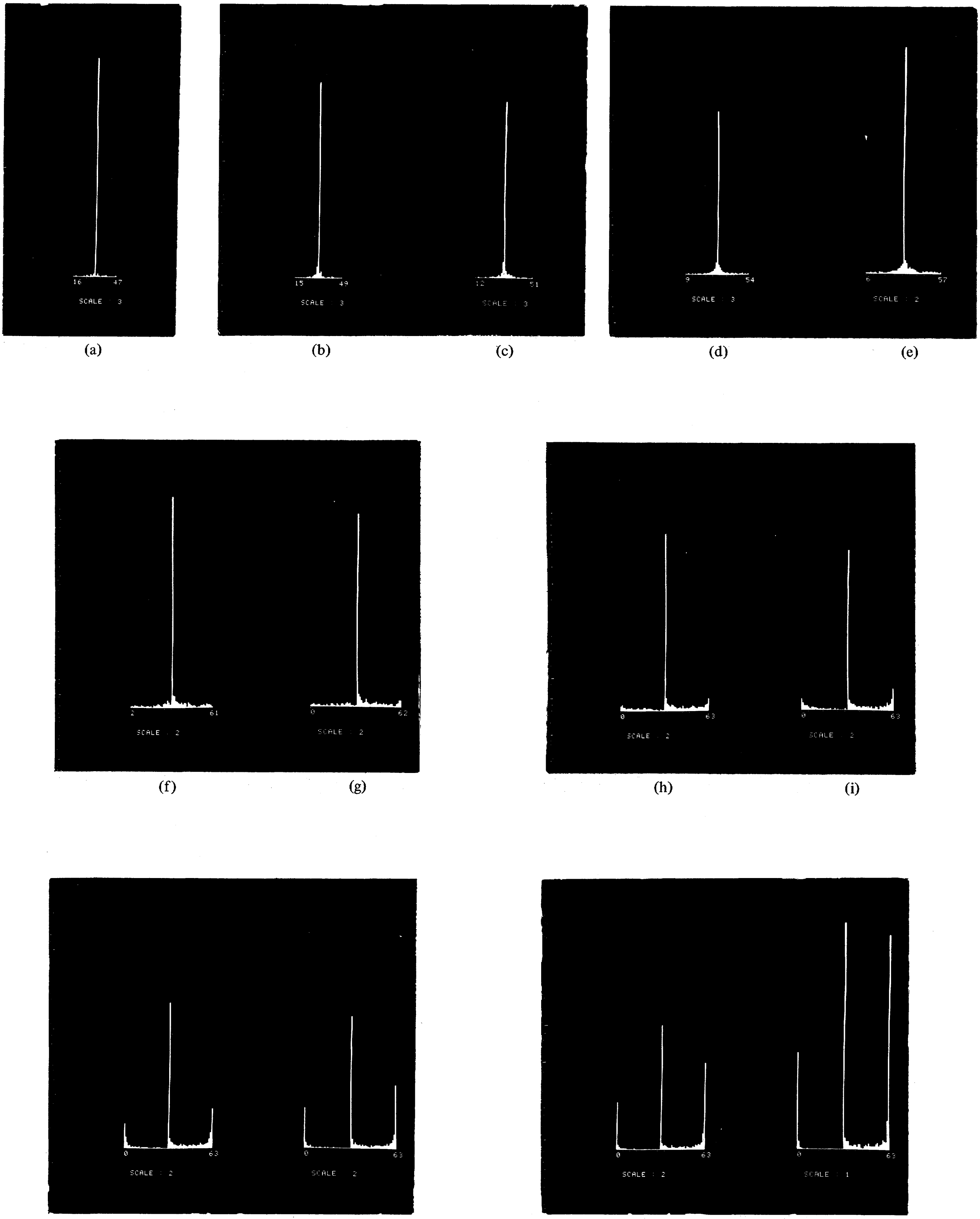

(a) (b) (c) (d) (e)

(f) (g) (h) (i)

(j) (k) (l) (m)

Fig. 17. (a)–(i) Histograms of Fig. 15(a)–(m).

pears to be choosing more intelligent coefficients to support the object information.

Using curvature to provide an initial estimate of inside/outside probabilities produced an accurate classification on our experimental curve. Now that we have verified its behavior, this information source should be brought to interact with the edge and gray level processes. The additional information should produce a still sharper object/background discrimination.

We also formulated a parallel model for computing compatibility coefficients for blob detection in a time sequence of images. We restricted motion to its simplest case, horizontal unit motion in one dimension, to study the object position/movement relations in successive frames. The model is untested as yet because of the computational cost involved. As the position/movement relations become better understood, they can be generalized to less restricted domains.

All of the processes examined in this paper are parallel processes. At present, the time requirements for these processes limit their usefulness as real-time object detectors. However, with the development of parallel processors the computational cost involved should well be within the requirements of real-time object detection.

Acknowledgment

The authors gratefully acknowledge the help of K. Riley in preparing this paper. Thanks are also due to C. Dyer for critical suggestions, R. Smith for his relaxation software and for implementing the borderness scheme, and S. Ranade for his efforts on the pyramid project.

References

[1] Zucker, "Relaxation labeling and the reduction of local ambiguities," in *Proc. 3rd Int. Joint Conf. Pattern Recognition*, San Diego, CA, Nov. 1976, pp. 852–861.

[2] Rosenfeld, "Iterative methods in image analysis," in *Proc. IEEE Conf. Pattern Recognition Image Processing*, New York, June 1977, pp. 14–18.

[3] Rosenfeld, Hummel, and Zucker, "Scene labeling by relaxation operations," *IEEE Trans. Syst., Man, Cybern.*, vol. SMC-6, pp. 420–433, 1976.

[4] Peleg, "A new probabilistic relaxation scheme," *IEEE Trans. Pattern Anal. Machine Intell.*, vol. PAMI-2, pp. 362–369, 1980.

[5] Peleg and Rosenfeld, "Determining compatibility coefficients for curve enhancement relaxation processes," *IEEE Trans. Syst., Man, Cybern.*, vol. SMC-8, pp. 548–555, 1978.

[6] Zucker, Krishnamurthy, and Haar, "Relaxation processes for scene labeling: Convergence, speed, and stability," *IEEE Trans. Syst., Man, Cybern.*, vol. SMC-8, pp. 41–48, 1978.

[7] Eklundh and Rosenfeld, "Convergence properties of relaxation," Comput. Sci. Center, Univ. Maryland, Rep. TR-701, Oct. 1978.

[8] Peleg and Rosenfeld, "Breaking substitution ciphers using a relaxation algorithm," *Commun. Ass. Comput. Mach.*, vol. 22, pp. 598–605, Dec. 1979.

[9] Peleg, "Ambiguity reduction in handwriting with ambiguous segmentation and uncertain interpretation," *Comput. Graphics Image Processing*, pp. 235–245, 1979.

[10] Davis and Rosenfeld, "Curve segmentation by relaxation labeling," *IEEE Trans. Comput.*, vol. C-26, pp. 1053–1057, 1977.

[11] Danker and Rosenfeld, "Strip detection using relaxation," *Pattern Recognition*, vol. 12, pp. 97–100, 1980.

[12] Schachter, Lev, Zucker, and Rosenfeld, "An application of relaxation methods to edge reinforcement," *IEEE Trans. Syst., Man, Cybern.*, vol. SMC-7, pp. 813–816, 1977.

[13] Peleg and Rosenfeld, "Straight edge enhancement and mapping," Comput. Sci. Center, Univ. Maryland, Rep. TR-694, Sept. 1978.

[14] Milgram, "Region extraction using convergent evidence," in *Proc. Image Understanding Workshop*, Apr. 1977, pp. 58–64.

[15] —, "Progress report on segmentation using convergent evidence," in *Proc. Image Understanding Workshop*, Oct. 1977, pp. 104–108.

[16] Rosenfeld and Kak, *Digital Picture Processing*. New York: Academic, 1978.

[17] Nakagawa and Rosenfeld, "Edge/border coincidence as an aid in edge extraction," *IEEE Trans. Syst., Man, Cybern.*, vol. SMC-8, pp. 899–901, 1978.

[18] Parikh and Rosenfeld, "Automatic segmentation and classification of infrared meteorological satellite data," *IEEE Trans. Syst., Man, Cybern.*, vol. SMC-8, pp. 736–743, 1978.

[19] Hayes, "Reading handwritten words using hierarchical relaxation," Ph.D. dissertation, Dep. Comput. Sci., Univ. Maryland, College Park, 1979.

[20] Rutkowski and Rosenfeld, "A comparison of corner-detection techniques for chain-coded curves," Comput. Sci. Center, Univ. Maryland, Rep. TR-623, Jan. 1978.

[21] Smith, "General purpose software package for array relaxation," M.S. thesis, Dep. Comput. Sci., Univ. Maryland, College Park, 1979.

[22] Cornsweet, *Visual Perception*. New York: Academic, 1970.

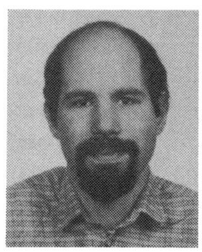

Alan J. Danker was born in Baltimore, MD, on November 24, 1952. He received the B.A. degree in English in 1975 and the M.S. degree in computer science in 1979, both from the University of Maryland, College Park.

In 1978 he was a Teaching Assistant at the University of Maryland. From 1978 to 1979 he was a Research Assistant at the Computer Vision Lab, also at the University of Maryland. He is currently with the Computervision Corp., Bedford, MA, working on a geometric database for a CAD/CAM graphics system. His present interests are in image processing and understanding, and artificial intelligence.

Mr. Danker is a member of the Association for Computing Machinery.

Azriel Rosenfeld (M'60–F'72), for a photograph and biography, see this issue, p. 11.